Phys Chem Minerals (2001) 28: 685–692

ORIGINAL PAPER

S. Heinemann · R. Wirth · G. Dresen

Synthesis of feldspar bicrystals by direct bonding

Received: 19 February 2001 / Accepted: 16 May 2001

Abstract We have produced synthetic feldspar bicrystals using a direct bonding technique. A gem-quality orthoclase crystal from Itrongay, Madagascar, was used for the bonding experiments. Microprobe analysis shows only minor concentrations of iron and sodium. Orthoclase single crystal plates oriented parallel (0 0 1) were cut and chemomechanically polished with silica slurry. From interferometry, final roughness of the square crystal plates was about 0.34 nm. Specimens were wet-chemically cleaned using deionised water. The bonding procedure produced an orthoclase bicrystal with an optically straight grain boundary-oriented parallel (0 0 1), which was investigated by HREM. Along the interface no amorphous layer was observed between lattice fringes of both crystals. We suggest that the bicrystals formed by initial hydrogen bonding and subsequent water loss and polymerisation of silanol and aluminol groups at elevated temperatures.

Key words Bicrystal synthesis · Feldspar · Direct bonding · Grain boundary

Introduction

A grain boundary may be defined as the zone separating two crystals differing in crystallographic orientation, composition or dimension of the crystal lattice (McLean 1957). In polycrystalline, multiphase materials grain boundaries or phase boundaries are present in a large number of configurations. The interfaces form three-dimensional networks very much like the networks of liquid films that constitute foams. The physical properties of grain boundaries, like their energy, resistivity and diffusivity, control the bulk physical properties of rocks. Most of our present knowledge on grain boundaries comes from studies of metals and alloys (e.g. Gleiter and Chalmers 1972; Sutton and Balluffi 1995). Likewise, the structure and properties of grain or phase boundaries in ceramics consisting of complex ionic and covalent compounds are also well investigated (e.g. Yan and Heuer 1983; Pask and Evans 1987; Wolf and Yip 1992; Tomsia and Glaeser 1998).

Compared to metals and ceramics, however, the chemical and mineralogical composition of silicate rocks is much more complex. Still relatively few studies exist that investigate the structure of grain boundaries in natural or synthetic rocks. The importance of grain or phase boundaries for rocks has been pointed out in several papers covering topics like the structure of grain boundaries (White and White 1981; Lee et al. 1984; Wirth 1986; Hay and Evans 1988; Bons et al. 1990; Renard and Ortoleva 1997; Hiraga et al. 1999), diffusion in grain boundaries (Nagy and Giletti 1986; Joesten 1991; Eiler et al. 1992; Fisler et al. 1997), impurity segregation (Byerly and Vogel 1973), chemically induced grain boundary migration (Evans et al. 1986) and metamorphism (Wada et al. 1998). Melt films along grain or phase boundaries indicating a possible amorphous structure of the grain or phase boundaries have been observed in natural mantle-derived xenoliths and in experimentally deformed rocks (Drury and Gerald 1996; Wirth 1996; de Kloe et al. 2000).

Friedel (1926) proposed the earliest model of a geometric interface. In general, structure and energy of a grain boundary depend on the orientation relationship of the two neighbouring grains. From observations in metals and ceramics and theoretical estimates of grain-boundary energy, two types of grain boundaries are commonly defined. Low-angle or subgrain boundaries separate domains of the same crystal with a misorientation <10°–15°. Grain-boundary energy increases with increasing misorientation. High-angle or simply grain boundaries separate individual crystals with a misorientation of >10°–15°. The energy of a high-angle grain boundary is largely independent of the crystal lattice

S. Heinemann (✉) · R. Wirth · G. Dresen
GeoForschungsZentrum Potsdam, Telegrafenberg D426,
14473 Potsdam, Germany
Tel.: +49-331-288 1323 Fax: +49-331-288 1328
e-mail: stefan.Heinemann@gfz-potsdam.de

orientation. However, it is reduced for special coincidence boundaries.

Several models of grain-boundary structure have been put forward. For example, it has been suggested that along grain boundaries no long-range order exists. The material along the boundary is essentially amorphous and comparable to a melt (Gleiter 1977; Wolf 1991; Keblinski et al. 1997). Recently, melt films with a minimum width down to 1 nm have been reported from olivine grain boundaries of mantle-derived xenoliths (Wirth 1996).

Low-angle grain boundaries may be formed by an array of dislocations ending in the boundary (dislocation model). However, interaction and overlap of dislocation cores with increasing misorientation between crystal domains severely complicate an atomistic approach. Bollmann (1970) suggested a geometric description of a grain boundary introducing the coincidence site lattice (CSL). Alternatively, Gleiter and Chalmers (1972) proposed that the boundary region formed by a periodic array of structural units.

In the core of the grain boundary, the average coordination number of atoms is reduced and the average bond length is changed compared to a regular crystal lattice. This requires elastic and plastic relaxation of the crystal lattice along a grain boundary on the atomic scale and compensation of resulting electric charges. The structural rearrangement commonly produces an excess free volume at the boundary. This structural difference with respect to the regular lattice and the charge compensation affect the grain boundary physical and chemical properties.

A systematic study of the structure and transport properties of grain boundaries requires a technique to fabricate synthetic bicrystals. The aim of this paper is to report such a technique for the preparation of K-feldspar bicrystals with a well-defined orientation relationship of the two grains.

Single crystals and bicrystals of silicates and most minerals cannot be grown from a melt, in contrast to metals. To produce a feldspar bicrystal, a contact between two single crystals is required on the atomic level. Therefore crystal surfaces have to be flat within a few atomic units. If surface roughness is too large, insufficient contact area develops. Contamination of surfaces with dust particles or adsorbates like hydrocarbons has to be avoided during preparation. For some materials the application of high temperatures and pressures (5–20 kbar, 600–1000 °C), resulting in plastic deformation of asperities, can overcome the detrimental effects of surface roughness (Christofferson et al. 1983; Snow and Kidman 1991). However, the direct bonding technique (Plößl and Kräuter 1999; Tong and Gösele 1999) does not require plastic deformation, and formation of primary dislocations near the interface is avoided, making this method especially suitable for brittle materials. Direct bonding requires careful preparation of the surfaces (Haisma et al. 1995) and an ultra-clean environment (Plößl and Kräuter 1999). To avoid contamination with adsorbates, sample preparation may be performed in ultrahigh vacuum (Fischmeister et al. 1992; Campbell 1996). An alternative preparation method is to saturate the crystal surface with suitable adsorbates. At elevated temperature the adsorbed material readily evaporates, leaving a contaminant-free boundary behind (Stengl et al. 1989). Adsorbates at silicate surfaces are mainly hydrocarbons and water. Both can produce a contact by hydrogen bonds at room temperature. However, hydrocarbons decompose at high temperatures, and decrepitation of trapped inclusions possibly affects the newly formed interface (Tong et al. 1995). However, water evaporates from an interface without decomposing, leaving an intact grain boundary behind (Plößl and Kräuter 1999).

Starting material and preparation

For the bonding experiments we used a gem-quality orthoclase crystal with yellowish colour from Itrongay, Madagascar (Gebrüder Bank, Idar-Oberstein, Germany). Orthoclases from Itrongay are low-sanidines (Nyfeler et al. 1998). The crystals are free of twins, exsolution lamellae and inclusions. Microprobe analysis shows only minor concentrations of iron and sodium: $K_{0.928(8)}Na_{0.053(2)}Al_{0.946(15)}Fe_{0.049(14)}Si_{3.021(5)}O_{8.024(7)}$. The lattice parameters were determined by powder X-ray diffraction in transmission mode: $a = 8.584(1)$ Å, $b = 13.006(3)$ Å, $c = 7.190(1)$ Aring;, ß = 116.016(7)°. The crystal is monoclinic because the characteristic (131) reflection shows no splitting.

Orthoclase single-crystal plates ($4 \times 4 \times 1$ mm, $15 \times 15 \times 0.5$ mm) oriented with X-ray diffraction parallel (0 0 1) were cut with an accuracy better than 0.5°. The (0 0 1) faces of the square plates were chemomechanically polished with a silica slurry (pH = 11) (CRYSTAL, Berlin). The final root-mean-square roughness of the crystal plates is 0.34 nm. The roughness was measured without contacting the surface, using interferometry (Kugler KMS microscope).

Synthesis of bicrystals by direct bonding

The specimens were wet-chemically cleaned in a clean room (class 100). Water was de-ionised using Millipore to give a resistivity of 18 MΩ. Subsequently, the water was quartz-filtered. Wet-chemical cleaning was performed in an ultrasonic bath in five steps with different chemicals. For each step the crystals were contained in a new Teflon cup (5–10 min). We used tweezers with platinum tips to handle the specimens.

For the cleaning of the crystal surfaces we applied a modified RCA1 solution (0.25 vol NH_4OH 29% + 1 vol H_2O_2 30% + 5 vol H_2O) (Radio Corporation of America; Kern and Puotinen 1970; Tong et al. 1995) and a standard RCA2 solution (1 vol HCl 37% + 1 vol H_2O_2 + 6 vol H_2O) combined with per-iodic acid.

In the first step, possible leaching of K, Na and Al from feldspar at low pH (RCA2) or alkali ammonium exchange at high pH (RCA1) was avoided by further modification of the solutions RCA1 and RCA2 to form a single hydrogen per-oxide cleaning solution (2 vol H_2O_2 30% Suprapur Merck + 13 vol H_2O, pH ~ 6.5) at 80 °C.

In the second step, per-iodic acid cleaning (10 g H_5IO_6 99.999% Aldrich + 1l H_2O, pH ~ 1) was applied to crack organic adsorbates (Tong et al. 1995).

In steps 3 and 4, acetone (99.9%, Uvasol, Merck) and isopropanol (99.9%, Uvasol, Merck) cleaning were performed. Finally, a H_2O bath was applied.

The crystal plates were removed from the water bath in a clean room (class 10), and then dried in a flow of N_2 (99.999%). To

establish the first contact of the two crystal surfaces, slight pressure was applied using the platinum-tipped tweezers (ca. 15 s). The contact area remained bonded after pressure was released. The contact geometry was a twist boundary with a rotation angle of 180° ± 3° and 169° ± 3° parallel to (0 0 1) for the small and large crystals, respectively. The couples were heated in a vacuum furnace at 400 °C and 10 Pa for 1 week. Finally, the $4 \times 4 \times 1$ mm^3 bicrystals were annealed at 1060 °C for up to 4 weeks and slowly cooled(5 °C min^{-1}) to ambient temperature. The $15 \times 15 \times 0.5$ mm^3 bicrystals started to cleave perpendicular to the interface at ~450 °C and annealing was stopped at 600 °C. Cleavages closed below 150 °C, but reappeared upon heating above 150 °C.

TEM

The $4 \times 4 \times 1$ mm^3 bicrystals were cut parallel to the interface and glued into a slit of an Al_2O_3 ceramic specimen holder (Strecker et al. 1993). Subsequently, slices were cut from this assembly and dimpled (GATAN) from both sides to a thickness of 15 μm. Finally, the specimens were ion-milled (GATAN Duomill; 5 kV, 11°) and carbon-coated.

TEM, HREM and analytical electron microscopy (AEM) were performed in a Philips CM200 microscope equipped with LaB_6 filament and GATAN imaging filter (GIF). For AEM an energy-dispersive X-ray analyser with ultrathin window was used. EDX analysis was performed in scanning mode using a window of 100×400 nm, reducing mass losses significantly.

The observed sensitivity of the specimen to electron irradiation damage was overcome by using the CCD camera of the GIF, which allowed exposure times of only 1–2 s. All of the HREM images are energy-filtered by applying a 10-eV slit to the zero loss peak.

Results

The bonding produced an orthoclase bicrystal with an optically straight grain boundary-oriented parallel (0 0 1). The HREM image in Fig. 1 shows a section perpendicular to the grain boundary, (0 1 0). Rotating the two crystals by 180° parallel (0 0 1) results in a Manebach twin. Close examination of this twin geometry reveals that the twin is equivalent to a near-coincidence lattice Σ4 (0 0 1) (Σ even is possible for non-cubic materials: King and Singh 1994).

No amorphous layer was observed between lattice fringes of both crystals along the interface. For both crystals, the *a* direction of the lattice is oriented parallel to the trace of the boundary. The zone axes are [0 1 0] and [0 $\bar{1}$ 0] respectively. The [1 0 2] direction (trajectory of ($\bar{2}$ 0 1) and (0 1 0) plane) of both crystals is inclined to the interface. The d_{001} lattice fringe spacing parallel to the grain boundary remains constant in vicinity to the grain boundary. The interface exhibits steps with the height of one d_{001} (= 0.69 nm) plane spacing (Fig. 2). In TEM the electron beam rapidly damages these areas. The resulting amorphous volumes with a diameter of a few nanometer show a regular spacing of about 30 nm to 35 nm along the interface. The network of secondary interface dislocations shown in Fig. 3 possibly compensates for a deviation from the 180° twist angle.

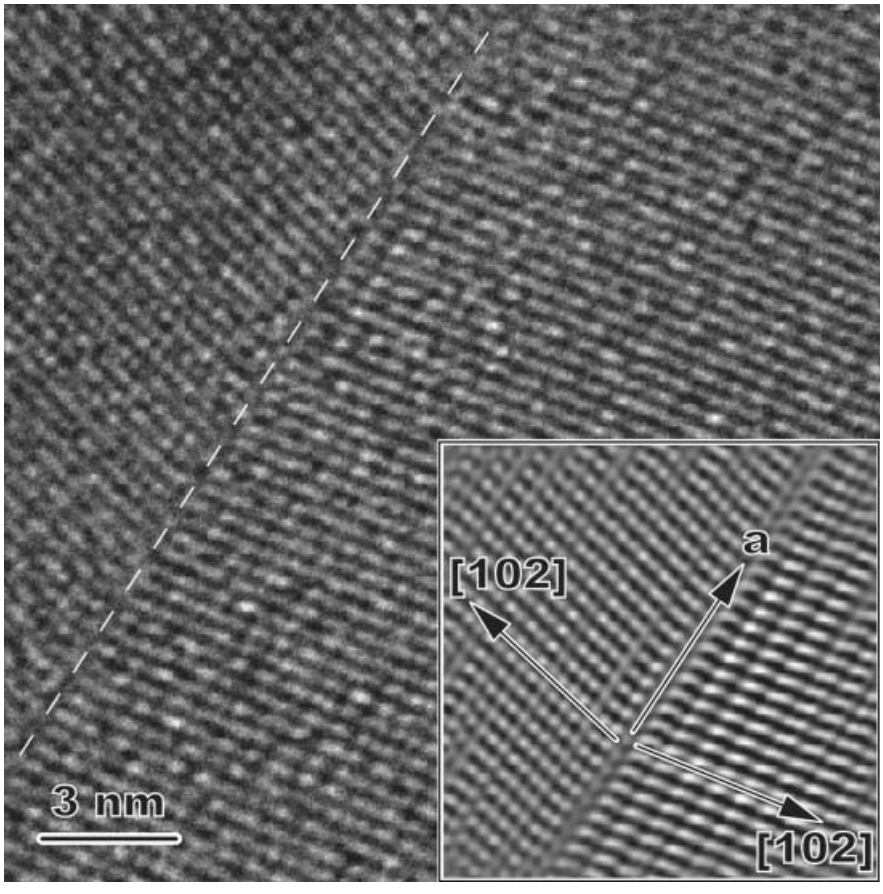

Fig. 1 Energy-filtered HRTEM image of synthesised orthoclase interface (interface perpendicular to the image). The area shows no defects along the coherent twin boundary. *Insert* is a Fourier-filtered image (FFT). The trace of the boundary is parallel to the *a* direction

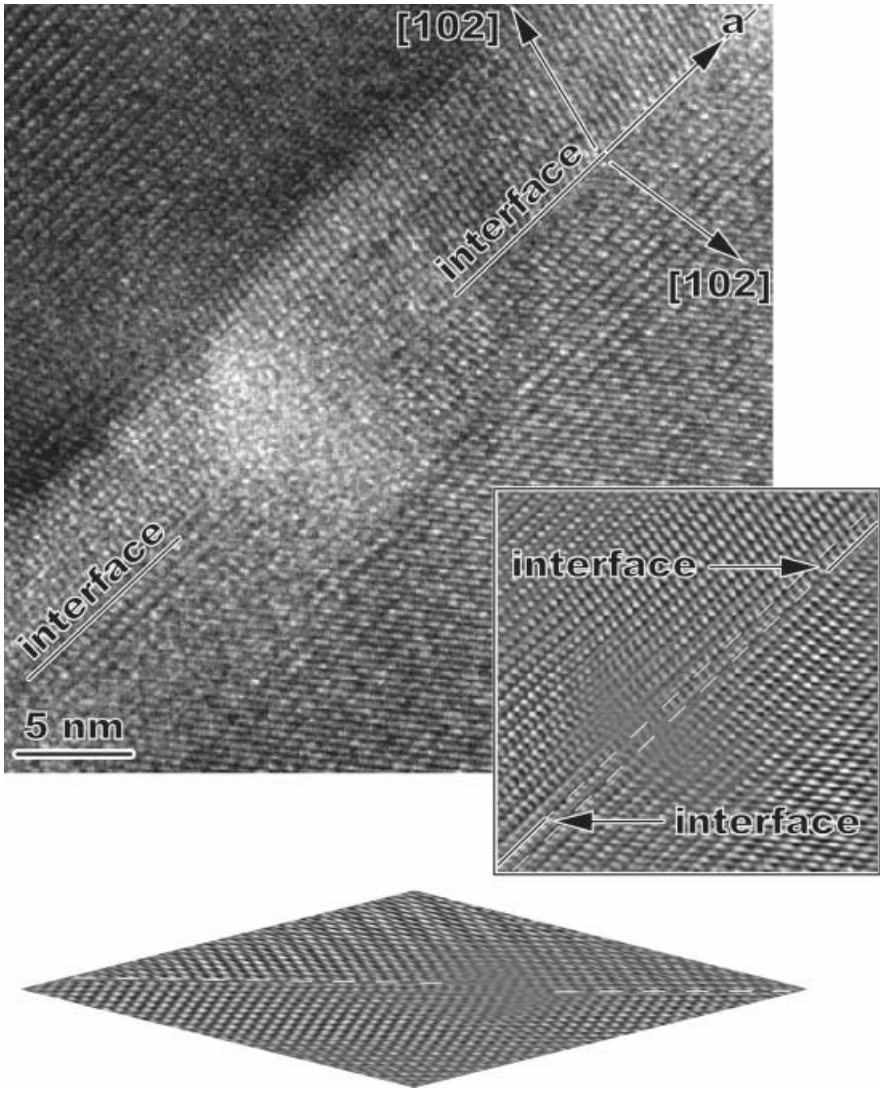

Fig. 2 The energy-filtered HRTEM image shows a step in the grain boundary between the orthoclase crystals (interface perpendicular to the image). In the *inserted* Fourier-filtered (FFT) image the interface is marked with *broken lines*. The *lower insert* is an oblique projection of the FFT image. *Broken lines* mark the interface left and right of the step

Chemical composition within 50 nm perpendicular to the grain boundary is similar to the neighbouring crystals (Table 1). The chemical composition measured by AEM agrees with the analysis performed in the electron microprobe.

Discussion

Formation of a proton-enriched surface layer and cation leaching

Feldspar surfaces exposed to air were found to adsorb various types of molecules such as carbon-enriched material, water and CO_2 (Wollast and Chou 1992; Nyfeler et al. 1997; Biino and Gröning 1998). Farquhar et al. (1999) found that molecular water is readily adsorbed on polished and cleaned (0 0 1) oligoclase feldspar surfaces. To achieve a water-saturated surface covered entirely by silanol and aluminol groups, hydrous cleaning in a bath of pure water is necessary. However, this procedure may affect the feldspar surface structure. Müller (1988) observed in $LiAlSi_3O_8$ feldspar cation exchange with protons, resulting in the formation of $HAlSi_3O_8$ feldspar. Cation-proton exchange in feldspars occurs at all pH conditions, and was found to increase with decreasing pH (Blum and Stilings 1995). Fenter et al. (2000) determined the structure of the (0 0 1) cleavage surface of an Itrongay orthoclase exposed to deionised water for 8 h. Only the outermost dangling cations at the surface are removed and the outermost surface consists of silanol and aluminol groups.

The comparison of the lattice spacings observed for our synthetic bicrystals with $HAlSi_3O_8$ (Deubener et al. 1991) do not indicate significant protonation of the near-surface region for the (0 0 1) crystal surfaces. Also, we did not observe amorphous layers along bicrystal interfaces after annealing at temperatures >500 °C, as might be expected for a strongly protonated material (Deubener et al. 1991). It is assumed that only the outermost dangling cations at the surface were exchanged with protons.

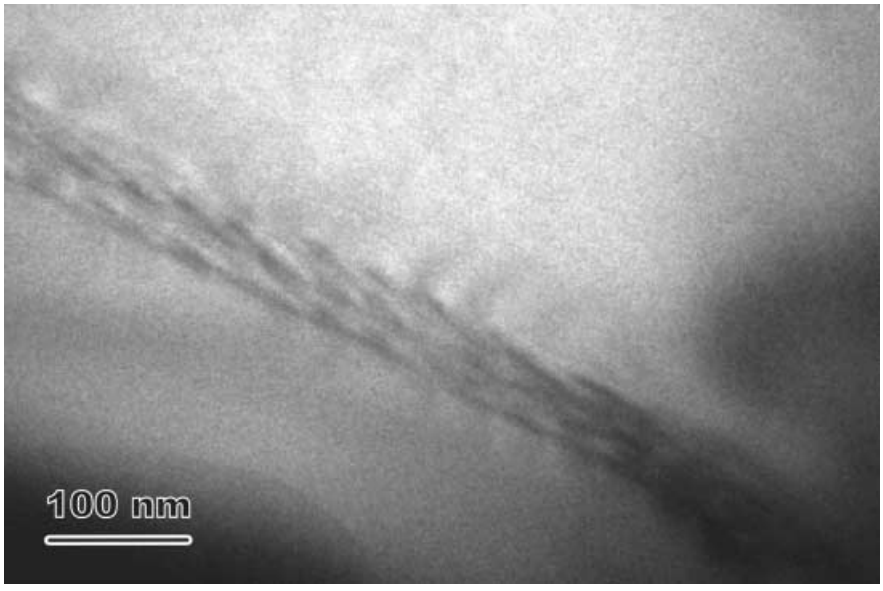

Fig. 3 TEM image of secondary interface dislocation network along the boundary of the orthoclase bicrystal. The image is a low-magnification overview of areas with and without defects displayed in Figs. 1 and 2

Table 1 Chemical composition of the single-crystal starting material (EMP) and the bicrystal (AEM)

Single-crystal orthoclase	$K_{0.928(8)}Na_{0.053(2)}Al_{0.946(15)}$ $Fe_{0.049(14)}Si_{3.021(5)}O_{8.024(7)}$
Bicrystal: off interface	$K_{0.960(18)}Na_{0.077(19)}Al_{0.905(12)}$ $Fe_{0.038(4)}Si_{3.035(10)}O_8$
Bicrystal: interface	$K_{0.953(80)}Na_{0.105(30)}Al_{0.929(47)}$ $Fe_{0.038(15)}Si_{3.011(40)}O_8$

In feldspar, preferred dissolution of aluminium, sodium and potassium, resulting in a depleted siliceous layer, requires a substantially longer exposure to water than required for surface protonation (Blum and Stilings 1995). In addition, acidic conditions with a pH <3–5 may be necessary (Blum and Stilings 1995). For example, Nesbitt et al. (1991) did not observe leaching of polished (0 0 1) faces of labradorite (An_{56}) in the pH range 4.05–5.6. Also, sanidine surfaces treated at a pH $= 1$ and a temperature of 150 °C for 1 h were not depleted in cations (Adriaens et al. 1999). Low pH conditions only existed during a short treatment of the bicrystals in a per-iodic acid bath (pH $= 1$, at 80 °C for 10 min).

In HREM observations of sanidine, a depleted siliceous layer was indicated by a breakdown of the feldspar framework (Adriaens et al. 1999). HREM images of the K-feldspar bicrystal interface presented here did not show any significant structural damage. Therefore, we do not expect that significant cation leaching occurred during preparation of the bicrystals.

Bonding model

Stengl et al. (1989) and Tong and Gösele (1999) suggested a direct bonding model for hydrophilic silicon wafers. The surface of hydrophilic Si wafers is covered with native amorphous silicon oxide. Carefully cleaned silicon wafers are usually covered exclusively with water molecules. The water is adsorbed by hydrogen bonding to silanol groups at the silica surface. At room temperature two Si wafers are spontaneously connected by hydrogen bonding between the absorbed water molecules. During thermal treatment of the wafers, molecular water escapes from the interface by grain-boundary diffusion and oxidation of silicon. Tong and Gösele (1999) suggested that hydrogen-bonded water at the interface is stable up to a temperature of 110 °C. For temperatures >110–150 °C, the fracture surface energy of the interface increases by almost an order of magnitude, but remains unchanged between 150 and 800 °C. Tong and Gösele (1999) proposed that an increase in bonding between 110 and 150 °C indicates a loss of molecular water and polymerisation of silanol groups to form siloxane bonds across the interface. Rangsten et al. (1999) applied this model to explain the bonding of quartz crystals. The rate-limiting step in direct bonding across the interface may be the closure of nanometer-sized voids by diffusion at high temperatures (>800 °C) (Derby and Wallach 1984; Orhan et al. 1999).

We suggest that the model for direct bonding of silicon wafers may be applied to explain the formation of feldspar bicrystals (Fig. 4). However, in contrast to silicon wafers, no spontaneous bonding between the feldspar surfaces occurred. Some force was initially required to keep the crystals in contact. Probably this resulted from a relatively large ratio of thickness to diameter and the high elastic rigidity of the feldspar samples compared to the silicon wafers.

We assume that silanol ≡Si–OH and aluminol ≡Al–OH groups and adsorbed water molecules cover the cleaned hydrophilic (0 0 1) surfaces of orthoclase (Fig. 4). For a polished and cleaned (0 0 1) oligoclase surface, Farquhar et al. (1999) found a thickness of the adsorbed water layer of 0.13 nm. The adsorbed water layer of a cleaved (0 0 1) Itrongay-orthoclase surface is

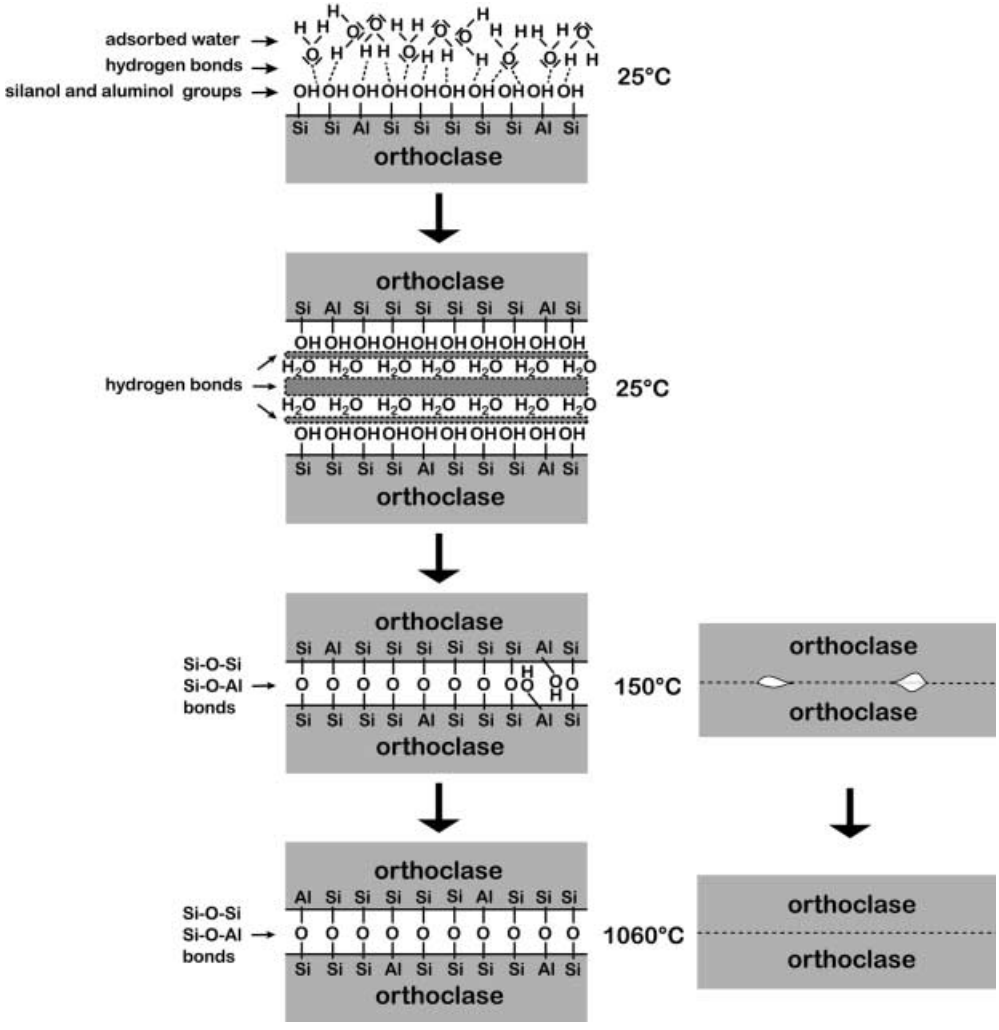

Fig. 4 Cartoon illustrating individual stages in direct bonding of feldspar crystals. At room temperature, hydrogen bonds form between opposing crystal surfaces that are initially covered with silanol and aluminol groups and adsorbed water molecules. Loss of water and polymerisation of silanol and aluminol groups occur at annealing temperatures of about 150 °C. Rearrangement of aluminium and silicon along the interface and the closure of voids requires relatively high temperatures of about 1000 °C

0.15 nm thick (Fenter et al. 2000). Presumably no ≡Si–OK and ≡Al–OK groups are present on the surface, because here protons readily exchange cations. Across the interface of the orthoclase bicrystal, initial hydrogen bonds exist between adsorbed water molecules, suggesting the reactions:

$$\equiv\text{Si–OH}\cdots\text{H}_2\text{O} + \text{H}_2\text{O}\cdots\text{HO–Si}\equiv \rightarrow \equiv\text{Si–OH}\cdots\text{H}_2\text{O}\cdots\text{H}_2\text{O}\cdots\text{HO–Si}\equiv$$
$$\equiv\text{Si–OH}\cdots\text{H}_2\text{O} + \text{H}_2\text{O}\cdots\text{HO–Al}\equiv \rightarrow \equiv\text{Si–OH}\cdots\text{H}_2\text{O}\cdots\text{H}_2\text{O}\cdots\text{HO–Al}\equiv$$
$$\equiv\text{Al–OH}\cdots\text{H}_2\text{O} + \text{H}_2\text{O}\cdots\text{HO–Al}\equiv \rightarrow \equiv\text{Al–OH}\cdots\text{H}_2\text{O}\cdots\text{H}_2\text{O}\cdots\text{HO–Al}\equiv \quad .$$

In silicon wafer, water is removed between 110 and 150 °C by oxidation of silicon and formation of dissolved H_2 and diffusion of molecular water through the native silicon oxide. However, reduction of water cannot occur in feldspar, and water molecules probably escape to the surface by migrating along the interface and by volume diffusion. Infrared measurements of adularia have shown that molecular water is removed from the crystal by diffusion in the temperature range 500–900 °C (Kronenberg et al. 1996). In the experiment presented here, the bonded feldspar crystals were heated to 400 °C in vacuum ($P = 10$ Pa) for 1 week to remove the water. Polymerisation of opposing silanol and aluminol groups will occur to form covalent bonds and water:

$$3\equiv\text{Si–OH} + \equiv\text{Al–OH} \rightarrow \equiv\text{Si–O Si}\equiv + \equiv\text{Si–O–Al}\equiv + 2\text{H}_2\text{O} \quad .$$

The bonding by polymerisation occurs at about 150 °C, as shown by thermally induced cleaving of the bicrystals. In the feldspar framework, bonding of two opposing AlO_4 tetrahedra is avoided for energetic reasons, and no ≡Al–O–Al≡ bindings form at adjacent aluminol groups. Phillips and Kirkpatrick (1995) suggested that the Al-avoidance rule (Loewenstein 1954) may possibly be violated to a small extent in anorthite at elevated temperatures only. Temperatures > 800 °C are required to rearrange opposing non-bonding Al tetrahedra by diffusion of Si and Al and to close voids related to surface roughness.

Conclusions

Direct bonding produced orthoclase bicrystals with optically straight grain boundaries oriented parallel (0 0 1). Rotating two crystals by 180° parallel (0 0 1) results in a Manebach twin with a near coincidence lattice of Σ4 (0 0 1). For both crystals the *a* lattice direction is oriented parallel to the boundary trace. A network of secondary interface dislocations possibly compensates for a deviation from the 180° twist angle. We have no indication for significant protonation and cation leaching in the near-boundary region. No amorphous layer was observed between lattice fringes of both crystals along the boundary. We suggest that direct bonding occurs in three steps with increasing annealing temperature. At room temperature hydrogen bonding connects the absorbed water layers, which are hydrogen bonded to the silanol and aluminol groups covering the crystal surfaces. At elevated temperature, water leaves the interface and Si/Al-tetrahedral groups connect across the boundary. At high temperatures, Al/Si interdiffusion may occur in the crystal lattice rearranging opposing Al/Si-tetrahedra and closing voids.

Acknowledgements We gratefully acknowledge the introduction into direct bonding of crystals by the research group of U. Gösele at MPI Halle, especially G. Kräuter and A. Plößl. We thank M. Rühle and J. Mayer, S. Hutt, A. Strecker and U. Salzberger at MPI, Stuttgart, for their support and valuable advises in preparing TEM sections of bicrystals.

References

Adriaens A, Goossens D, Pijpers A, Van Tendeloo G, Gijbels R (1999) Dissolution study of potassium feldspars using hydrothermally treated sanidine as an example. Surf Interface Anal 27: 8–23

Biino GG, Gröning P (1998) X-ray photoelectron spectroscopy (XPS) used as a structural and chemical surface probe on aluminosilicate minerals. Eur J Mineral 10: 423–437

Blum AE, Stilings LL (1995) Feldspar dissolution kinetics. In: White AF, Branzly SL (eds) Chemical weathering rates of silicate minerals. Rev Mineral 31: 291–351

Bollmann W (1970) Crystal defects and crystalline interfaces. Springer, Berlin Heidelberg New York

Bons AJ, Drury MR, Schryvers D, Zwart HJ (1990) The nature of grain boundaries in slates. Phys Chem Miner 17: 402–408

Byerly GR, Vogel TA (1973) Grain-boundary processes and development of metamorphic plagioclase. Lithos 6: 183–202

Campbell GH (1996) Σ5 (210)/[001] Symmetric tilt grain boundary in yttrium aluminium garnet. J Am Ceram Soc 79: 2883–2891

Christofferson R, Yund RA, Tullis J (1983) Inter-diffusion of K and Na in alkali feldspars; diffusion couple experiments. Am Mineral 68: 1126–1133

Derby B, Wallach ER (1984) Diffusion bonding: development of theoretical model. Metal Sci 18: 427–431

Deubener J, Sternitzke M, Müller G (1991) Feldspars $MalSi_3O_8$ (M = H,Li,AG) synthesized by low-temperature ion-exchange. Am Mineral 76: 1620–1627

Drury MR, Fitz Gerald DF (1996) Grain boundary melt films in upper mantle rocks. Geophys Res Lett 23: 701–704

Eiler JM, Baumgartner LP, Valley JW (1992) Intercrystalline stable isotope diffusion: a fast grain boundary model. Contrib Mineral Petrol 112: 543–557

Evans B, Hay RS, Shimizu N (1986) Diffusion-induced grain-boundary migration in calcite. Geology 14: 60–63

Farquhar ML, Wogelius RA, Tang CC (1999) In-situ synchrotron X-ray reflectivity study of the oligoclase feldspar mineral-fluid interface. Geochim Cosmochim Acta 63: 1587–1594

Fenter P, Teng H, Geissbühler P, Hanchar JM, Nagy KL, Struchio NC (2000) Atomic-scale structure of the orthoclase (001)–water interface measured with high-resolution X-ray reflectivity. Geochim Cosmochim Acta 64: 3663–3673

Fischmeister HF, Elssner G, Gibbesch B, Kadow KH, Kawa F, Korn F, Mader W, Turwitt M (1992) Solid-state bonding of accurately oriented metal/ceramic bicrystals in ultrahigh vacuum. Rev Sci Instrum 64: 234–242

Fisler DK, Mackwell SJ, Petsch S (1997) Grain boundary diffusion in enstatite. Phys Chem Miner 24: 264–273

Friedel G (1926) Leçons de cristallographie 2nd edn. Berger-Levraux, Paris

Gleiter H (1977) Korngrenzen in metallischen Werkstoffen. Materialkundlich Technische Reihe 2, Borntraeger, Stuttgart

Gleiter H, Chalmers B (1972) High-angle grain boundaries. Prog Mater Sci 16, Pergamon Press, New York

Haisma J, Spiercings GACM, Michielsen TM, Adema CL (1995) Surface preparation and phenomenological aspects of direct bonding. Philips J Res 49: 23–46

Hay RS, Evans B (1988) Intergranular distribution of pore fluid and the nature of high-angle grain boundaries in limestone and marble. J Geophys Res B93: 8959–8974

Hiraga T, Nagase T, Akizuki M (1999) The structure of grain boundaries in granite-origin ultramylonite studied by high-resolution electron microscopy. Phys Chem Miner 26: 617–623

Joesten R (1991) Grain boundary diffusion kinetics in silicate and oxide minerals. In: Ganguly J (ed) Diffusion, atomic ordering, and mass transport: selected problems in geochemistry. Springer, Berlin Heidelberg New York, pp 345–395

Keblinski P, Phillpot SR, Wolf D, Gleiter H (1997) Amorphous structures of grain boundaries and grain junctions in nanocrystalline silicon by molecular dynamics simulations. Acta Mater 45: 987–998

Kern W, Puotinen DA (1970) Cleaning solutions based on hydrogen peroxide for use in silicon semiconductor technology. RCA Review 30: 187–206

King AH, Singh A (1994) Generalising the coincidence site lattice model to non-cubic materials. J Phys Chem Solids 55: 1023–1033

Kloe de R, Drury MR, van Roermund HLM (2000) Evidence for stable grain boundary melt films in experimentally deformed olivine-orthopyroxene rocks. Phys Chem Miner 27: 480–494

Kronenberg AK, Yund RA, Rossman GR (1996) Stationary and mobile hydrogen defects in potassium feldspar. Geochem Cosmochem Acta 68: 4075–4094

Lee JH, Peacor DR, Lewis DD, Wintsch RP (1984) Chlorite-illite/muscovite interlayered and interstratified crystals: a TEM/STEM study. Contrib Mineral Petrol 88: 372–385

Loewenstein W (1954) The distribution of aluminium in the tetrahedra of silicates and aluminates. Am Mineral 39: 92–96

McLean D (1957) Grain boundaries in metals. Oxford University Press, London

Müller G (1988) Preparation of hydrogen and lithium feldspars by ion exchange. Nature 32: 435–436

Nagy KL, Giletti BJ (1986) Grain boundary diffusion of oxygen in microperthitic feldspar. Geochimica Cosmochimica Acta 50: 1151–1158

Nesbitt HW, Macrae ND, Shotyk W (1991) Congruent and incongruent dissolution of labradorite in dilute, acidic salt solutions. J Geol 99: 429–442

Nyfeler D, Berger R, Gerber (1997) Scanning force microscopy on albite cleavage surfaces. Schweiz Mineral Petrogr Mitt 77: 21–26

Orhan N, Aksoy M, Eroglu M (1999) A new model for diffusion bonding and its application to duplex alloys. Mater Sci Eng A271: 458–468

Pask JA, Evans AG (1987) Ceramic microstructures 86: role of interfaces. Material Sci Research vol 21, Plenum Press, New York, pp 985

Phillips BL, Kirkpatrick RJ (1995) High-temperature 29 Si MASNMR spectroscopy of anorthite (CaAl2Si2O8) and its P$\bar{1}$–I$\bar{1}$ structural phase transition. Phys Chem Miner 22: 269–276

Plößl A, Kräuter G (1999) Wafer direct bonding: tailoring adhesion between brittle materials. Mat Sci Eng R25: 1–88

Rangsten P, Vallin Ö, Hermansson K, Bäcklund Y (1999) Quartz-to-quartz direct bonding. J Electrochem Soc 146: 1104–1105

Renard F, Ortoleva P (1997) Water films at grain-grain contacts: Debye-Hückel, osmotic model of stress, salinity, and mineralogy dependence. Geochim Cosmochim Acta 61: 1963–1970

Snow E, Kidman S (1991) Effect of fluorine on solid state alkali interdiffusion rates in feldspar. Nature 349: 231–233

Stengl R, Tan T, Gösele U (1989) A model for the silicon wafer bonding process. Jpn J Appl Phys 28: 1735–1741

Sutton AP, Balluffi RW (1995) Interfaces in crystalline materials. Monographs on the physics and chemistry of materials, 51. Clarendon Press, Oxford

Tomsia AP, Glaeser AM (1998) Ceramic microstructures: control at the atomic level. Proceedings International Materials Symposium Ceramic Microstructures '96, Berkeley, California, Plenum Press, New York

Tong QY, Gösele U (1999) Semiconductor wafer bonding. Wiley, New York

Tong QY, Kaido G, Tong L, Reiche M, Shi F, Steinkirchner J, Tan TY, Gösele, U (1995) A simple chemical treatment for preventing thermal bubbles in silicon wafer bonding. J Electrochem Soc 42: L201–L203

Wada H, Ando T, Suzuki M (1998) The role of the grain boundary at chemical and isotopic fronts in marble during contact metamorphism. Contrib Mineral Petrol 132: 309–320

White JC, White SH (1981) On the structure of grain boundaries in tectonites. Tectonophysics 78: 613–628

Wirth R (1986) High-angle grain boundaries in sheet silicates (biotite/chlorite): a TEM study. J Mat Sci Lett 5: 105–106

Wirth R (1996) Thin amorphous films (1–2 nm) at olivine grain boundaries in mantle xenoliths from San Carlos, Arizona. Contrib Mineral Petrol 124: 44–54

Wolf D (1991) A model for ideal cleavage fracture of grain boundaries in b.c.c. metals. Phil Mag A 63: 1117

Wolf D, Yip S (1992) Materials Interfaces: atomic level structure and properties. Chapman and Hall, London

Wollast R, Chou L (1992) Surface reactions during the early stages of weathering of albite. Geochim Cosmochim Acta 566: 3113–3122

Yan MF, Heuer AH (1983) Character of grain boundaries. Advances in ceramics, vol 6. Am Cer Soc